Boron Nanowires for Flexible Electronics and Field Emission

Jifa Tian, Jinming Cai, Chao Hui, Chen Li, Yuan Tian, Chengmin Shen and Hongjun Gao

Institute of Physics, Chinese academy of Sciences, Beijing 100190, P R China

Abstract. Development of a rational synthetic method of flexible nanomaterials may enable exciting avenues in both fundamental research and novel device applications. In this paper, flexible boron nanowires have been successfully synthesized on both Si (111) and scanning tunneling microscope (STM) tungsten (W) tips via thermoreduction of boron-oxygen compounds with active metal (magnesium). These as-prepared nanowires, which are structurally uniform and single crystalline, represent good semiconductor at high temperature. Electrical conductivity of these intrinsic nanowires can be improved two orders by introducing doping atoms. Tensile stress measurements demonstrate excellent mechanical property of as-synthesized boron nanowires as well as resistance to mechanical fracture even under a strain of 3%. Importantly, simultaneous electrical measurement reveals that the corresponding electrical conductance is very robust and remains constant under mechanical strain. Our results can be briefly explained by Mott's variable range hopping (VRH) model. A stable field emission current was also observed from a single boron nanowire. Boron nanostructures with excellent controllability, remarkable mechanical flexibility and field emission characteristics represent promising candidates for flexible nanoelectronic circuits as well as electron emission nanodevices.

Keywords: Boron, Nanowires, Single crystalline, Electronics, Flexibility, Field emission.
PACS: 61. 62. Km; 62. 23. Hj; 68. 37. Og; 73.63-b

INTRODUCTION

Analogues to the revolutionary miniaturization in electronic industry initiated in 1950s, flexible electronics might also change the world in the future[1]. While recent rapid progress has been achieved in flexible technology[2, 3], one major technological challenge is to seek a suitable material that can retain excellent electrical performance even under large mechanical strain. Recently, significant efforts have been applied to two different types of flexible nanomaterials: inorganic semiconductors and organic conducting materials. The high-performance inorganic electronic materials, such as silicon tend to fracture under 1% tensile strain. While single-walled carbon nanotubes have shown great promise for applications in flexible electronics, ill- control of structural chirality make them a big challenge for being useful in high-performance integrated circuits[1, 3].

Among well-known light elements such as B, C, N,[4-7] boron possesses many unique properties. Similar to carbon and silicon, boron shows an obvious tendency to form covalent molecular compounds, but differs dramatically from C in having one less valence electron than the number of valence orbitals, a situation sometimes referred to be "electron deficiency"[8]. Boron not only is the third lightest solid element with a low density of 2.340 g/cm^3 and a high melting point of 2300 °C, but also has large bulk young's modulus of 380-400 GPa, and extreme hardness close to diamond. These unique mechanical and electronic features make boron and its related compounds promising for future applications in flexible technology. Particularly, recent theoretical work on boron and AlB_2 nanotubes[9, 10] have stimulated significant experimental interest.

So far, different techniques have been developed to fabricate one dimensional (1D) boron nanostructures. Amorphous boron nanowires were successfully fabricated by chemical vapor transport[5], radio-frequency magnetron sputtering[11, 12], or laser ablation technique[13]. Ill- defined crystalline boron nanowires were directly synthesized by chemical vapor deposition reaction of diborane (B_2H_6) in Ar gas[14]. Tetragonal and rhombohedral boron nanostructures have been realized by laser ablation and thermal vapor transport process, respectively[15-18]. Recently, boron nanocones have been successfully synthesized via thermal evaporation of B/B_2O_3 precursors in an Ar/H_2 gas mixture in our group[19]. Nevertheless, due to the

low productivity and poor quality of the boron nanowires, detailed characterization of their physical properties has been lack[14, 20]. In this article, we will highlight the synthesis method, describe the related fabrication technical issues, and outline their properties for flexible electronics and field emission applications.

THE FABRICATION AND CHARACTERIZATION OF BORON NANOWIRES

Synthesis of Single Crystalline Boron Nanowires and Device Fabrication

Our work was based on a new synthetic route to grow single crystalline boron nanowires on Si (111) and STM W tips through active metal (magnesium) thermal reduction of B/B_2O_3 in a H_2/Ar mixture gas at $1000 \sim 1200$ °C using Fe_3O_4 nanoparticles as catalyst. Fe_3O_4 nanoparticles with diameter of 6-8 nm were synthesized by high temperature solution phase reaction of iron (III) acetylacetonate with 1, 2-dodecandiol in the presence of oleic acid and oleylamine[21]. Boron powder (99.9%), boron oxide (B_2O_3) powder (99.99%) and magnesium (99.99%) in a molar ratio of 10:1:3 were grounded together as precursors and placed inside alumina boat. The Fe_3O_4 nanoparticles liquid-drops were added onto Si (111) wafer as the substrate. After drying, it was placed at the backward position which is about 2 cm away from the precursors in the reaction boat. A high temperature tube furnace (Lindberg/Blue STF54434C) with accurate control of temperature and gas flow rate was applied for synthesis boron nanostructures. Detailed growth conditions of boron nanowires are as follows. At first, 100 sccm H_2/Ar carrier gas was introduced after the system was pumped down to 10 Pa and the program for temperature controlling was started simultaneously. When the temperature of furnace center reached 400 °C at a rate of 200 °C/h, the system was kept for 30 min to eliminate remaining oleic acid and oleylamine on the surface of catalysts. Then, the flow rate of the carrier gas was decreased to 50 sccm and the system pressure was maintained at 3- 4 x 10^3 Pa. The system temperature was then heated to 1100 °C at a rate of 200 °C/h without changing the system pressure. Boron nanowires were grown under this condition for 2h. After that, the furnace temperature went down to room temperature at a rate of 200 °C/h. Finally, dark brown or black products were found on the surface of the substrate. In order to measure the field emission properties of a single boron nanowire,

we grew nanowires directly onto W tips. These W tips were fabricated by an electrochemical etching method using NaOH solution, and then were dipped into the Fe_3O_4 catalyst solution. After drying, they were placed at the backward position which is about 1.5 cm away from the precursors in the reaction boat. The remaining growth process was the same as that of boron nanowires on silicon substrates.
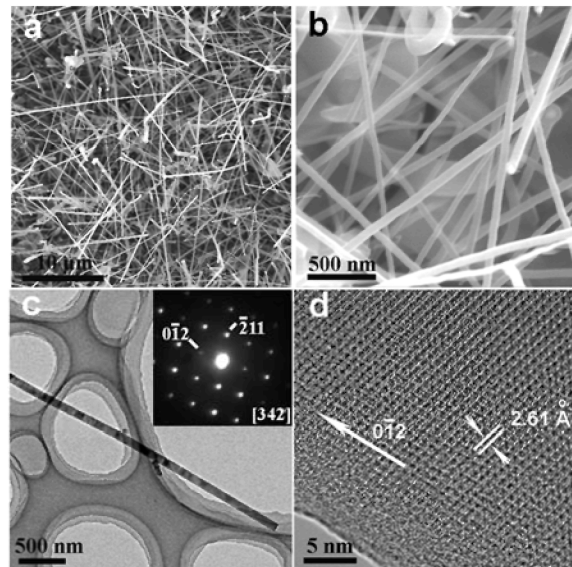

FIGURE 1. Structural characterizations of boron nanowires. a, SEM image of boron nanowires on Si (111) substrate showing as-synthesized boron nanowires are tens of micrometers long with large quantity. b, High resolution SEM image of boron nanowires showing that the diameter of boron nanowires ranges from 50 to 200 nm. c, Typical TEM image of a single boron nanowire. The inset is the corresponding SAED pattern which can be indexed to β - Rhombohedral boron. d, HRTEM image of boron nanowire with clear lattice fringe. The growth direction is along [$0\bar{1}2$] and the measured lattice distance is about 2.16 Å, agreeing with ($\bar{2}03$) lattice plane.

Morphologies of boron nanowires were examined by field-emission type scanning electron microscope (FESEM) (XL-SFEG, FEI Corp.). Transmission electron microscope (TEM) (Tecnai-20, PHILIPS Cop.) and high-resolution transmission electron microscope (HRTEM) (Tecnai F20, FEI Corp.) with electron energy loss spectrometer (EELS) were employed to perform the microanalysis of boron nanowires. Crystal structure was determined by x-ray diffraction (XRD) (D/Max-2400). The contact electrodes of boron nanowire device 1 were fabricated by electron beam lithography (EBL) (Raith 150, Raith company, Germany). The detailed fabrication processes are as follows: firstly, boron nanowires were dispersed in ethanol with ultrasonic process; then, the boron

318

nanowires suspension solution was dropped on a heavily doped thermally oxidized Si (111) wafer with a thickness of 500 nm SiO_2 on the top. Four contact electrode patterns were defined on PMMA 950 using E-beam and followed by thermal evaporation Ni/Au (20/130 nm) and lift-off. For comparison, four Pt (100 nm) Ohmic contact electrodes on a single boron nanowires were also fabricated by focused ion bean (FIB) (DB 235, FEI, USA).

Electrical transport, flexibility and field emission measurements were conducted using our home-made four-probe STM system[22]. This four-probe STM not only provides four exact localizers, but also gives four electrodes. The field emission property of single nanowire can be measured by using two probes and the field emission property on single oscillatory nanowire also can be performed by introducing a electrical field on one side of nanowire using other two probes. Therefore, the four-probe STM provides a powerful tool to study the field emission measurements on individual nanowire.

The Characterization of Boron Nanowires

We recently developed a novel synthetic route for pure β-Rhombohedral boron nanowires following vapor-liquid-solid (VLS) process. Typical morphologies and micro-structure of boron nanowires are shown in Fig. 1. These nanowires are about tens of micrometers long and 50-200 nm wide, with random growth angles to the substrate (Fig. 1a, b). More detail structure of nanowires can be characterized by transmission electron microscopy (TEM) and selected area electron diffraction (SAED), further revealing crystalline lattice fringes without observable defects.
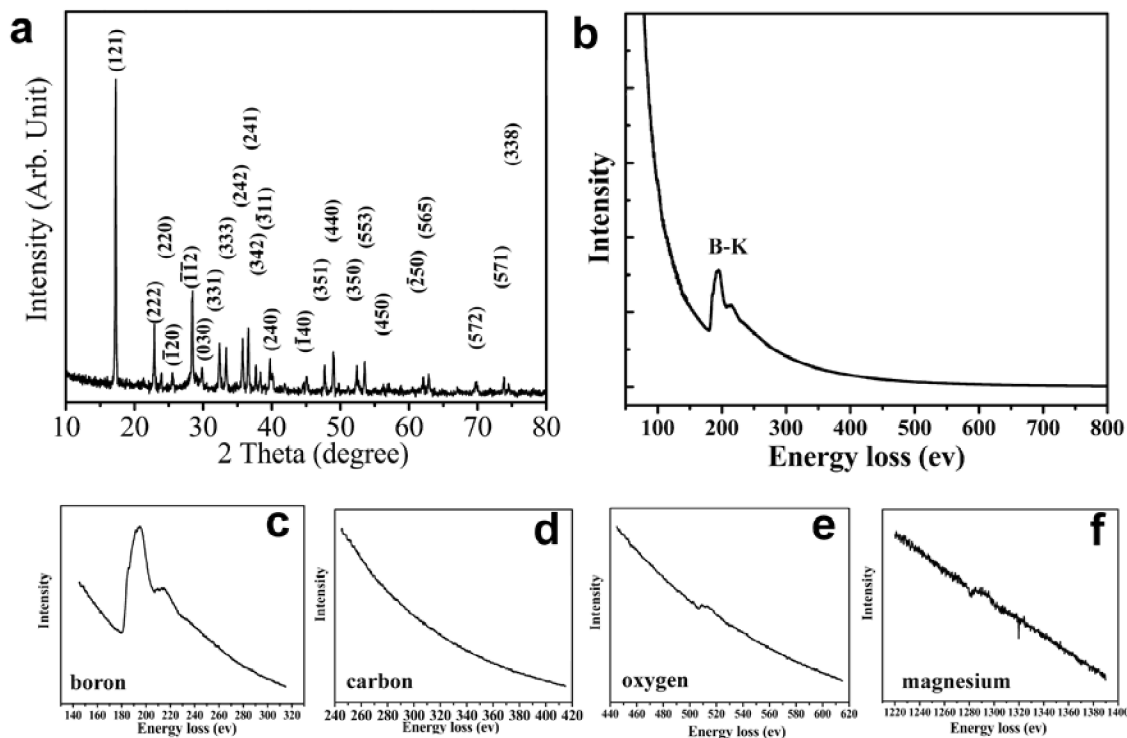

FIGURE 2. a, The XRD spectra of the synthesized boron nanowires. b, A typical EELS spectrum from individual nanowire. c, A peak corresponding to the K-shell ionization edge of the boron is clearly seen at about 188 eV. d, e, f, The EELS for possible impurities of carbon (283 eV), oxygen (532 eV) and magnesium (1305 eV), respectively.

The X-ray diffraction spectroscopy of as-grown products is shown in Fig. 2a. It can be seen that the diffraction peaks are sharp and narrow. These peaks, which match well with the standard result (JCPDS card no.: 85-0409), were indexed on the basis of rhombohedral-centered boron. Thus, it has been further demonstrated that the products are pure β-Rhombohedral boron nanowires. The chemical compositions of single boron nanowires were analyzed by electron energy loss spectroscopy (EELS). Figure 2b-f shows the typical EELS spectrum of the nanowire. The characteristic B K-edge at 188 eV is clearly visible and no other peaks can be distinguished in Fig. 2b. The other possible existing elements (carbon, oxygen and magnesium) also have been well identified (Fig. 2d-f). The signals of carbon and magnesium are

too weak to be detected by the limitation of EELS. There is a very weak peak of O K-edge at 532eV (Fig. 2e). It is due to the oxidation of boron at the nanowire surface.
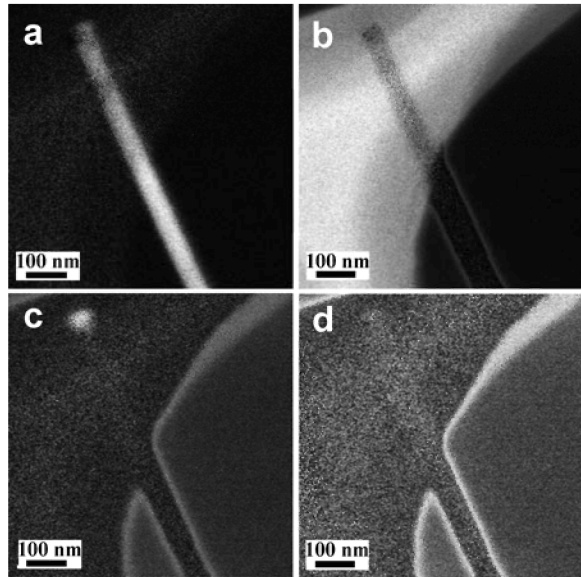

FIGURE 3. Elemental mappings of boron nanowires. a, boron. b, carbon. c, iron and d, oxygen.

In order to further confirm the element distribution in the nanowires, the energy filter transmission electron microscope (EFTEM) was introduced into the investigation. The energy filter mapping image of boron (Fig. 3a) exhibits that it uniformly located in the nanowire. From the mapping image of carbon in Fig. 3b, it can be seen that carbon only appears at the film on the grid and there is no carbon appeared at the location of the nanowire. Figure 3c is the energy filter mapping image of iron, which only exists at the tip of the wire. So it can be concluded that the growth process of boron nanowires follows vapor-liquid-solid (VLS) mechanism. There is no evidence which indicates the existence of oxygen in Fig. 3d. But combining the EELS data and the reported results, we can see that boron can be oxidated after exposed in the air. By the numbers of investigation, it can be concluded that the prepared wires are pure boron nanowires.
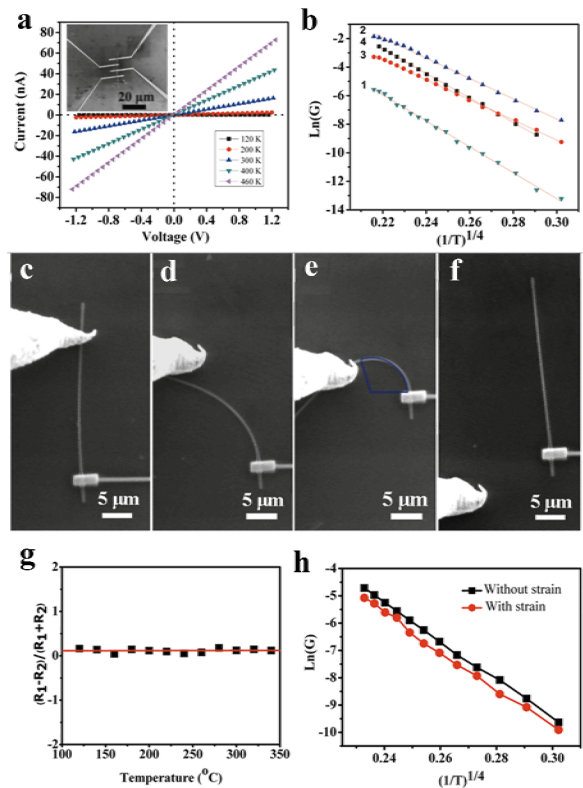

FIGURE 4. Electrical transport measurement of single boron nanowire. a, I-V characterization of boron nanowire with Ni/Au electrodes measured from 120 K to 460 K. The inset gives the SEM image of EBL fabricated four-electrode device with a single 120 nm boron nanowire . b, Temperature dependence of electrical conductivities of four different devices. The indiced numbers of each curve represent the names of the devices described in the main text. c-f SEM images showing mechanical bending process. g, The relationship between $(R_1-R_2)/(R_1+R_2)$ and temperature T. h, Temperature dependence of conductivities of nanowires with and without mechanical strain.

PROPERTIES INVESTIGATION ON BORON NANOWIRES

The Electrical and Mechanical Properties of a Single Nanowire

Figure 4a shows current versus bias voltage (I-V) characteristics of single boron nanowire measured under different temperatures. All of the I-V curves are linear and symmetrical under a bias voltage up to 10 V (not show here), and the conductance increases with the temperature. At 460 K the conductance can be improved by 3 orders as compared with that of 120 K, indicating that boron nanowire is a good semiconductor above room temperature. The electrical

conductivity of device 1 is about 4.4×10^{-4} $(\Omega\cdot cm)^{-1}$ at room temperature, which is close to the value of bulk boron $(10^{-4}\sim10^{-7})^{23}$. For comparison, device 2 was made by EBL but it was fixed with Pt by FIB at the contacts between boron nanowire and the electrodes. The conductivities of device 2 is 3.6×10^{-2} $(\Omega\cdot cm)^{-1}$ which is 2 order higher than that of device 1. The same behavior was also observed in device 3 and 4 which were realized by FIB using Pt as the electrodes. Such conductivity enhancement can be attributed to the doping atoms (Ga and Pt) introduced in the FIB process.

Figure 4b gives linear relationships between Ln(G) and $(1/T)^{1/4}$ of these four devices. Here G is the conductivity and T is the temperature. Such linear dependence can be understood by Mott's VRH model, assuming that the carrier transport occurs by thermal activation process between the localized states. According to the Mott's law for the three-dimensional VRH, the conductivity G is expressed as:

$$G = G_0 \exp\left\{-\left(\frac{T_0}{T}\right)^{1/4}\right\} \qquad (1)$$

$$T_0 = \frac{60}{\pi k_B l^3 N(E_F)} \qquad (2)$$

Where l is the localization length of the carrier's wave function, $N(E_F)$ is the electron density of (localized) states at the Fermi level (E_F). k_B is the Boltzmann constant, and G_0 is constant. Our data agree with this model well.

We further observed that the conductance of boron nanowires was very robust even under large strain. In this experiment, one of the tips in our four-probe apparatus was used as both electrode (in a two terminal configuration) and manipulator (Fig. 4c- f) so that the electrical conductance can be monitored during the bending process. The mechanical strain of nanowire experienced can be quantized as $\varepsilon = r/R$, where r and R represent the nanowire's radius and the radius of curvature, respectively, and can be directly measured by SEM. The nanowire remains intact even after 3% strain bending (Fig. 4e), which manifests excellent resilence as compared with single crystal bulk counterpart. Importantly, the resistance of boron nanowire is very robust and remains almost unchanged while increasing the strain step by step by the tip. The resistivities measured under the situation of Fig. 4c-e are 139.3, 143.8, 142.4 $\Omega\cdot cm$, respectively. The variation of resistivities might be due to different contact conditions during the electrode fabrication process. Figure 4g shows independence of $(R_1-R_2)/(R_1+R_2)$ on temperature T, where R_1, R_2 are the resistances of boron nanowire without strain and with 3% strain, respectively. This independence of

electrical conductance on mechanical strain can also be directly seen in the Fig. 4h. Our observed temperature dependent transport process of boron nanowire with strain also agrees well with the Mott's VRH mechanism. Compared with the result of curve without strain (slope is -70.4), the slope under the strain was almost the same (-70.31), which further suggest that strain on boron nanowires didn't change its electron density of (localized) states at the Fermi level. Our results of robust electrical conductance of boron nanowires suggest that it might be an excellent candidate for flexible electric device.
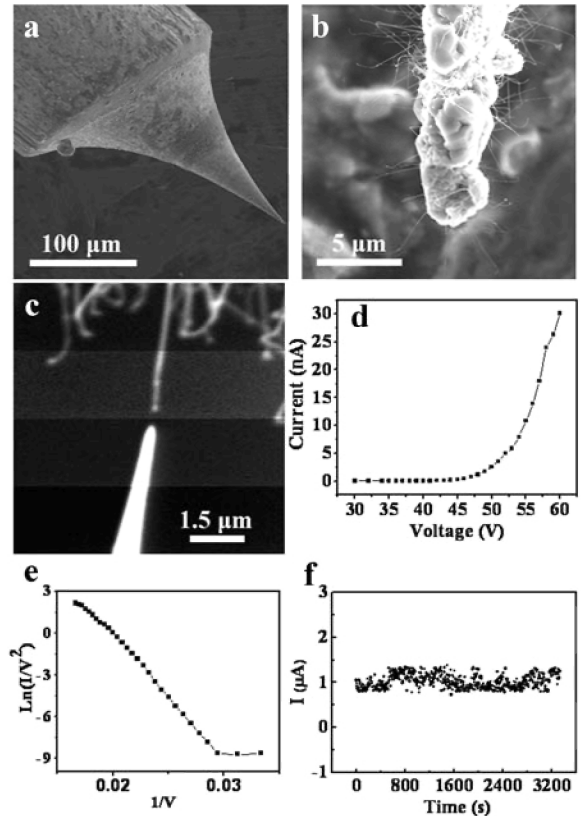

FIGURE 5. Field emission characteristics of a single boron nanowire. a, Typical SEM image of a STM W tip. b, High magnification SEM image of the tip showing lots of the boron nanowire grown on the tip apex. c, Field emission measurement by the four-probe STM system. The two electrodes are the prepared W tips. The distance between two electrodes is ~ 300 nm. d, I-V characteristics of the field emission measurement performed on the boron nanowire. e, The corresponding F-N plot of the I-V curve. f, The field emission stability curve of an individual boron nanowire at high emission current.

The Field Emission Properties of a Single Boron Nanowire

We further investigated potential applications of as-synthesized boron nanowire on field emission. In order to study the field emission property, boron nanowires were directly grown onto a STM W tip apex, and the field emission current from a single nanowire can be measured by using another probe as electrode. Figure 5 details the field emission measurement processes as well as typical results from single boron nanowire. Figure 5a exhibits that the boron nanowires were directly synthesized on a STM W tip. In higher magnification SEM images (Fig. 5b), it can be seen that lots of nanowires have been successfully synthesized on the surface of the STM tip. This prepared tip and another clean tip were used as the cathode and anode, respectively, which can be manipulated exactly as shown in Fig. 5c. The distance and the angle between nanowire and the STM W tip can be determined in an accurate manner (Fig. 5c). Figure 5d shows emission current-voltage (I-V) characteristics of a boron nanowire with ~ 80 nm in diameter and several micrometers long under an inter-electrode distance of 300 nm. With this configuration, a field emitted current can be detected which shows a threshold voltage of 34 V. The emission current density is ~10^4 A/cm^2 at 60 V, which is better than those of other nanowires reported so far[24-26] and compatible to those of the multi-wall carbon nanotubes[27, 28]. The F-N plot, $\ln(I/V^2)$ vs. $1/V$, is shown in Fig. 5e. The good linearity of the plot suggests that the field emission from boron nanowire emitter agrees with a metal-vacuum field emission (F-N) model[29]. Measurements on different nanowires show consistent field emission characteristic as well as temperature stability.

Boron is one kind of negative temperature coefficient resistors, which can ensure that individual boron nanowire still has a good emission property at high temperature. Here we measure the emission stability of an individual boron nanowire at a direct current (DC) voltage of 200 V. Figure 5f is the representative emission stability curve of the nanowire at high current. The whole measurement lasts for about 1 hour. It can be seen that the boron nanowire exhibit a stable field emission at high current of 1.05 μA and only a fluctuation less than 23% occurs through the continuous high current operation. We can approximately calculate the emission temperature of individual boron nanowires at this measurement by one-dimensional thermal current density law on semiconductor transistor:

$$T_j = \frac{W}{\kappa A} P_c + T_a \qquad (3)$$

Where, T_j is the temperature of boron nanowire, T_a is the room temperature, W is adopted to be the length of nanowire, A is the heat-radiative area, P_C is the heating power on the nanowire, and κ is 27.4 W·m^{-1}·K^{-1}, which is the thermal conductivity of bulk boron materials. The shape of boron nanowire is thought to be columned, so the radiative area A is calculate by $A=2\pi r W$, where r and W is the mean radius and length of individual boron nanowire, respectively. Considering the heat-exchanging coefficient η of the input power P_I is 80%~90% in the field emission process, P_C is obtained by the relationship of $P_C=P_I\eta$. Base on the above-mentioned theory, the temperature of individual boron nanowire is calculated to be about 700~800 °C at the emission current of 1.01 μA, indicating it has good stable field emission properties at high temperature.

CONCLUSIONS

In summary, we have developed a novel synthetic route for making high quality boron nanowires.[29] The electrical transport of single boron nanowires shows room temperature conductivity of 4.4×10^{-4} (Ω • cm)$^{-1}$, and follows the Mott's VRH mechanism. This electrical conductivity is very robust under mechanical strain up to 3%. Field emission characteristic of individual boron nanowire reveal a stable and high field emission current density. We believe that all our results together suggest that boron nanostructures are promising nanoscale building blocks for flexible nanoelectronics as well as field emission nanodevices.

ACKNOWLEDGMENTS

REFERENCES

1. S. Hong and S. Myung, *Nature Nanotech.* **2**, 207-208 (2007).
2. Y. Sun, W. M. Choi, H. Jiang, Y. Y. Huang and J. A. Rogers, *Nature Nanotech.*, **1**, 201-207 (2006).
3. X. Lu and Y. Xia, *Nature Nanotech.* **1**, 163- (2006).
4. S. Iijima, *Nature* **354**, 56-58 (1991).
5. Y. Y. Wu, B. Messer and P. D. Yang, *Adv. Mater.* **13**, 1487-1489 (2001).
5. D. N. McIlroy, D. Zhang, R. M. Cohen and J. Wharton, *Phys. Rev. B* **60**, 4874-4879 (1999).

7. W. L. Wang, X. D. Bai, K. H. Liu, Z. Xu, D. Bolberg, Y. Bando and E. G. Wang, *J. Am. Chem. Soc.*, **128**, 6530-6531 (2006).

8. V. I. Matkovich, "Boron and refractory borides". Springer, New York, 1977.

9. A. Gindulyte, W. N. Lipscomb and L. Massa, *Inorg. Chem.* **37**, 6544-6545 (1998).

10. I. Boustani, A. Quandt, E. Hernandez and A. Rubio, *J. Chem. Phys.* **110**, 3176-3185 (1999).

11. L. M. Cao, Z. Zhang, L. L. Sun, C. X. Gao, M. He, Y. Q. Wang, Y. C. Li, X. Y. Zhang, G. Li, J. Zhang and W. K. Wang, *Adv. Mater.* **13**, 1701-1704 (2001).

12. L. M. Cao, K. Hahn, Y. Q. Wang, C. Scheu, Z. Zhang, C. X. Gao, Y. C. Li, X.Y. Zhang, L. L. Sun, W. K. Wang and M. Ruhle, *Adv. Mater.* **14**, 1294-1297 (2002).

13. X. M. Meng, J. Q. Hu, Y. Jiang, C. S. Lee and S. T. Lee, *Chem. Phys. Lett.* **370**, 825-828 (2003).

14. C. J. Otten, O. R. Lourie, M. F. Yu, J. M. Cowley, M. J. Dyer, R. S. Ruoff and W. E. Buhro, *J. Am. Chem. Soc.* **124**, 4564-4565 (2002).

15. Y. J. Zhang, H. Ago, M. Yumura, T. Komatsu, S. Ohshima, K. Uchida and S. Iijima, *Chem. Comm.* **23**, 2086-2087 (2002).

16. S. H. Yun, A. Dibos, J. Z. Wu and D. K. Kim, *Appl. Phys. Lett.* **84**, 2892-2894 (2004).

17. Z. K. Wang, Y. Shimizu, T. Sasaki, K. Kawaguchi, K. Kimura and N. Koshizaki, Chem. *Phys. Lett.* **368**, 663-667 (2003).

18. T. T. Xu, J. G. Zheng, N. Q. Wu, A. W. Nicholls, J. R. Roth, D. A. Dikin and R. S. Ruoff, *Nano Lett.* **4**, 963-968(2004).

19. X. J. Wang, J. F. Tian, T. Z. Yang, L. H. Bao, C. Hui, F. Liu, C. M. Shen, C. Z. Gu, N. S. Xu and H. J. Gao, *Adv. Mater.* 19, 4480-4485 (2007).

20. D. W. Wang, J. G. Lu, C. J. Otten and W. E. Buhro, *Appl. Phys. Lett.* **83**, 5280-5282 (2003).

21. T. Z. Yang, C. M. Shen, Z. A. Li, H. R. Zhang, C. W. Xiao, S. T. Chen, Z. C. Xu, D. X. Shi, J. Q. Li and H. J. Gao, *J. Phys. Chem. B*, **109**, 23233-23236 (2005).

22. X. Lin, X. B. He, T. Z. Yang, W. Guo, D. X. Shi, H. J. Gao, D. D. D. Ma, S. T. Lee, F. Liu and X. C. Xie, *Appl. Phys. Lett.* **89**, 043103-1 (2006).

23. *Landolt-bornstein numerical data and functional relationships*. New series, edited by H. H. Hellwege, Springer-verlag: Berlin, 1983, Vol. III/ 17e, pp. 16-18.

24. Y. Yu, C. H. Jin, R. H. Wang, Q. Chen and L. M. Peng, *J. Chem. Chem. B* **109**, 18772-18776 (2005).

25. Y. H. Huang, Y. Zhang, Y. S. Gu, X. D. Bai, J. J. Qi, Q. L. Liao and J. Liu, *J. Phys. Chem. C*, **111**, 9039-9043 (2007).

26. H. Zhang, J. Tang, Q. Zhang, G. P. Zhao, G. Yang, J. Zhang, O. Zhou and L. C. Qin, *Adv. Mater.* **18**, 87-91 (2006).

27. Z. Xu, X. D. Bai, E. G. Wang and Z. L. Wang, *Appl. Phys. Lett.* **87**, 163106-1-3 (2005).

28. J. M. Bonard, K. A. Dean, B. F. Coll, C. Klinke, *Phy. Rev. Lett.* **89**, 197602-1-4 (2002).

29. R. H. Fowler, L. W. Nordheim, Proc. Roy. Soc. A, 119 (1928) 173.

30. J. F. Tian, J.M. Cai, C. Hui, C. D. Zhang, L. H. Bao, M. Gao, C. M. Shen, and H.-J. Gao, *Appl. Phys. Letters* **93**, 122105-1-3, (2008).